HHS Public Access

Author manuscript

Adv Healthc Mater. Author manuscript; available in PMC 2016 January 07.

Published in final edited form as:

Adv Healthc Mater. 2015 January 7; 4(1): 131–141. doi:10.1002/adhm.201400129.

Gel Scaffolds of BMP-2-binding Peptide Amphiphile Nanofibers for Spinal Arthrodesis

Sungsoo S. Lee[#]
Department of Materials Science and Engineering, Northwestern University, Evanston, IL 60208, USA

Prof. Erin L. Hsu[#]
Department of Orthopaedic Surgery, Institute for BioNanotechnology in Medicine, Northwestern University, Chicago, IL 60611, USA

Dr. Marco Mendoza, **Dr. Jason Ghodasra**, **Dr. Michael S. Nickoli**, **Amruta Ashtekar**, **Dr. Mahesh Polavarapu**, **Dr. Jacob Babu**, **Dr. Rehan M. Riaz**, **Dr. Joseph D. Nicolas**, **Dr. David Nelson**, and **Sohaib Z. Hashmi**
Department of Orthopaedic Surgery, Northwestern University, Chicago, IL 60611, USA

Start R. Kaltz
Department of Materials Science and Engineering, Northwestern University, Evanston, IL 60208, USA

Dr. Jeffrey S. Earhart and **Prof. Bradley R. Merk**
Department of Orthopaedic Surgery, Northwestern University, Chicago, IL 60611, USA

Dr. Jeff S. McKee and **Dr. Shawn F. Bairstow**
Baxter international Inc., Deerfield, IL 60016, USA

Prof. Ramille N. Shah
Department of Materials Science and Engineering, Northwestern University, Evanston, IL 60208, USA

Department of Surgery, Institute for BioNanotechnology in Medicine, Northwestern University, Chicago, IL 60611, USA

Prof. Wellington K. Hsu
Department of Orthopaedic Surgery, Department of Neurological Surgery, Institute for BioNanotechnology in Medicine, Northwestern University, Chicago, IL 60611, USA

Prof. Samuel I. Stupp[*]
Department of Materials Science and Engineering, Department of Chemistry, Northwestern University, Evanston, IL 60208, USA

Department of Medicine, Institute for BioNanotechnology in Medicine, Northwestern University, Chicago, IL 60611, USA

[#] These authors contributed equally to this work.

[*] s-stupp@northwestern.edu.

Supporting Information Supporting Information is available online from the Wiley Online Library or from the author.

Abstract

Peptide amphiphile (PA) nanofibers formed by self-assembly can be customized for specific applications in regenerative medicine through the use of molecules that display bioactive signals on their surfaces. We report here on the use of PA nanofibers with binding affinity for the bone promoting growth factor BMP-2 to create a gel scaffold for osteogenesis. With the objective of reducing the amount of BMP-2 used clinically for successful arthrodesis in the spine, we used amounts of growth factor incorporated in the scaffolds that are 10 to 100 times lower than that those used clinically in collagen scaffolds. The efficacy of the bioactive PA system to promote BMP-2-induced osteogenesis *in vivo* was investigated in a rat posterolateral lumbar intertransverse spinal fusion model. PA nanofiber gels displaying BMP-2-binding segments exhibited superior spinal fusion rates relative to controls, effectively decreasing the required therapeutic dose of BMP-2 by ten-fold. Interestingly, a 42% fusion rate was observed for gels containing the bioactive nanofibers without the use of exogenous BMP-2, suggesting the ability of the nanofiber to recruit endogenous growth factor. Results obtained here demonstrate that bioactive biomaterials with capacity to bind specific growth factors by design are great targets for regenerative medicine.

Keywords

Peptide amphiphile; Spinal fusion; Bone regeneration; BMP-2 (bone morphogenetic protein-2); Regenerative medicine

1. Introduction

Pseudarthrosis--the non-union of bone in fractures, therapeutic bone fusions, or skeletal defects--remains a significant clinical challenge despite recent advances on implantable medical devices and use of biologics such as growth factors. In the United States alone, current estimates suggest that over 200,000 spine fusion procedures are performed annually with pseudarthrosis reported to be as high as 10–15% overall and as high as 48% in posterolateral inter-transverse process lumbar fusions [1,2]. In addition, approximately 6 million bone fractures are reported to occur annually with 10% resulting in delayed or impaired healing [2,3]. With increasing average life expectancy, the burden of musculoskeletal disease will become more prominent, and thus there is a great demand for improved treatment methods to maintain quality of life.

Recombinant human bone morphogenetic protein-2 (BMP-2) in combination with an absorbable type I collagen sponge is a bone graft substitute widely used in challenging healing environments such as osteoporosis, nonunion repair, and multilevel fusions. As a critical growth factor that greatly influences the osteoinductivity of bone grafts, BMP-2 delivered on a collagen sponge has demonstrated highly enhanced bone formation in long bone defect repairs and spinal arthrodesis [4]. However, efficient healing requires supraphysiologic doses of the cytokine, which may lead to surgical complications including bone resorption, graft migration, hematoma formation, radiculitis, and heterotopic ossification [5–9]. The challenges associated with the current use of BMP-2 have led to an extensive search for more optimal scaffolds that can reduce the therapeutic dose of the cytokine and thus lower the potential risks [10,11]. One proven approach is the development

of biomaterials that can release one or more growth factors with controlled kinetics [12–14]. In addition, recent efforts have been made to develop biomimetic materials that not only better retain the therapeutic agent, but also provide an artificial extracellular environment that mimics the endogenous healing process, thereby maximizing the bioactivity of the therapeutic [15–17].

Our laboratory has pioneered the use of peptide amphiphile (PA) molecules as building blocks to create biomaterials for regenerative medicine. These PAs are designed to self-assemble in aqueous conditions into high-aspect-ratio nanofibers that are biomimetic of extracellular filaments measuring approximately 10 nanometers in diameter and microns in length. Their formation is driven mainly by secondary interactions such as collapse of hydrophobic molecular segments away from an aqueous environment and hydrogen bonding among peptide segments leading to β-sheet secondary structure [18]. These supramolecular nanofibers are programmed to display a high surface density of biological cues and this way function as artificial extracellular matrices (ECM) for regenerative medicine [19]. Previous examples include repair of the central nervous system [20] and cartilage [21], neovascularization of ischemic heart tissue [22], enamel growth [23], and bone repair [24,25], among others. *In vivo*, gel scaffolds of PA nanofibers have shown desirable rates of biodegradation on the order of weeks [20,26].

In prior studies, PAs have also been utilized as therapeutic gels with prolonged release of growth factors [21,27,28]. Other groups have shown that heparan sulfate-like glycosaminoglycans (HSGAGs), which are rich in sulfo- and carboxyl-groups, bind and localize growth factors and enhance their signaling by facilitating ligand-receptor interactions [29,30]. Our laboratory previously designed a PA bearing a Cardin-Weintraub heparin-binding domain such that nanofibers formed by this molecule would bind HSGAGs, creating a biomimetic matrix. This heparin-binding PA (HBPA) gel exhibited substantial neovascularization in a rat cornea angiogenesis model using only nanogram quantities of angiogenic growth factors [27,31]. Interestingly, the HBPA-polysaccharide gel without exogenous growth factors was sufficient to promote the formation of new vasculature in a mouse dorsal skinfold chamber model [26]. Furthermore, the HBPA system exhibited enhanced bone regeneration with a high probability of bridging in a rat critical-size femur defect model using only 1 μg BMP-2, a dose that is less than one tenth of the required dose for union in that model [28]. In a separate study, we designed a PA with a binding segment to transforming growth factor β-1 (TGFβ-1) with the aim of creating a nanofiber matrix that could localize and recruit endogenous cytokine [21]. The supramolecular gel prepared by co-assembling this bioactive PA with a diluent PA that lacks the binding sequence promoted regeneration of articular cartilage in a rabbit chondral defect microfracture model even without the addition of exogenous TGFβ-1.

In the present study, we report on the development of a self-assembling PA system that can bind both endogenous and exogenous BMP-2 for use in bone regeneration. The PA molecule design contains a carboxyl-rich peptide domain (E_3) as well as a peptide segment with BMP-2-binding affinity, NH_2-TSPHVPYGGGS-COOH, which was identified previously in our laboratory using phage display [32]. This BMP-2-binding PA is evaluated co-assembled with negatively charged diluent molecules to space the BMP-2-binding

segment. *In vitro* studies were performed to investigate the influence of this PA system and suitable controls on BMP-2-induced differentiation of C2C12 pre-myoblasts into an osteogenic lineage. Furthermore, we tested *in vivo* the system's ability to promote osteogenesis in the clinically relevant procedure of spinal fusion, using a rat posterolateral lumbar intertransverse model.

2. Results

2.1. Design and characterization of the BMP-2-binding PA

The BMP-2-binding PA (BMP2b-PA) was designed to display a BMP-2-binding peptide sequence on the surface of the nanofibers (Figure 1). Since phage-displayed peptides are linked via the C terminus, we covalently attached at this terminus a carboxyl-rich E_3 domain and an A_3V_3 β-sheet-forming domain, followed by a terminal lysine with a C_{12} alkyl chain linked to the ε-amino group (Figure 1A). This sequence is used to promote supramolecular self-assembly into cylindrical nanofibers. The diluent PA was designed without the bioactive segment and contains only the E_3 domain linked at the N terminus a A_3V_3 β-sheet-forming domain, followed by a C_{16} alkyl chain (Figure 1A). The alkyl lengths of the two PAs were selected to match the length of the hydrophobic moieties of these two molecules. Repeated units of valines and alanines found in the BMP-2-binding PA and the diluent PA have been shown to promote self-assembly of other PA molecules into nanofibers via β-sheet formation along the length of the fibers [33]. Here, our circular dichroism (CD) studies verified that both PAs exhibited spectra that are indicative of β-sheets with a maximum near 195 nm and a minimum near 216 nm (Figure 1B). The β-sheet signature of the diluent PA was red-shifted, a feature associated with twisting of the secondary structure [33]. The BMP-2-binding PA and the diluent PA were co-assembled in aqueous conditions to form the diluted BMP-2-binding PA (D-BMP2b-PA), which should display the binding segment on the nanofiber surface with higher accessibility to the protein than the BMP-2-binding PA alone (Figure S1 of the Supporting Information (SI)). Cryogenic transmission electron microscopy (cryo-TEM) revealed the formation of self-assembled cylindrical nanofibers for the diluent PA, BMP-2-binding PA, and the diluted BMP-2-binding PA (Figure 1C). The diluent PA formed high-aspect-ratio nanofibers measuring microns in length, whereas the BMP-2-binding PA formed nanofibers with submicron lengths. When these two PAs were co-assembled at 1:1 weight ratio, we also observed high-aspect-ratio cylindrical nanofibers.

To assess PA nanofiber stability, we measured the critical micelle concentration (CMC) of PAs by Nile red fluorescent probe assay [34]. At pH 7.4, the supramolecular assembly of the BMP-2-binding PA was detected at above 666 nM (1.5 μg/mL), and that of the diluent PA was detected at above 1 μM (1.2 μg/mL) (Figure S2 of the SI). We also investigated the binding affinities of the PAs to BMP-2 by surface plasmon resonance (SPR) using hexahistidine-tagged BMP-2 (His-BMP-2) that was immobilized on the surface via nickel (II)-nitrilotriacetic acid (Ni^{2+}-NTA) chelation [35]. As a control, the BMP-2-binding PA (1 μM, pH 7.4) was injected to a bare NTA-dextran chip, and we observed non-specific binding of the PA to the surface (Figure S3 of the SI). We speculate that the fibrillar nanostructures can be entangled to the NTA-dextran surface. To circumvent this, we prepared the BMP-2-binding PA at pH 8.4, where more glutamic acid residues will be deprotonated to induce

greater electrostatic repulsion between the PA molecules, and sonicated the solution to further break up the supramolecular assembly. Consequently, the CMC measurements of the two PAs revealed disruption of the assembly at pH 8.4 (Figure S2). This BMP-2-binding PA prepared at pH 8.4 also showed minimal binding to the NTA-dextran surface (Figure S3). Hence, for the SPR analysis, we immobilized His-BMP-2 on the Ni^{2+}-NTA surface at pH 7.4 and injected the BMP-2-binding PA or the diluent PA solutions that were prepared at pH 8.4 (Figure 2). The best fit was obtained by using the 2:1 binding model, which had two dissociation constants: a major dissociation constant ($k_{d,1}$) and a minor dissociation constant ($k_{d,2}$) with the ratio of their contributions (R_1/R_2). By using the major dissociation rate and the association rate (k_a), we found that the BMP-2-binding PA had a lower K_D (3.7×10^{-8} M) than the diluent PA (2.1×10^{-6} M), suggesting a higher binding affinity to BMP-2.

2.2. PA nanofibers in solution enhance BMP-2-induced osteogenesis *in vitro*

C2C12 pre-myoblast cells have been used as a model to probe the mechanism by which extracellular components such as heparin or heparan sulfate potentiate BMP-2-induced osteoblast differentiation [36,37]. In this study, we used C2C12 cells to investigate the ability of PA nanofibers to modulate BMP-2 activity *in vitro* (Figure 3). We also used porcine heparin as a positive control. Initial studies verified that the diluent PA, the BMP-2-binding PA, the diluted BMP-2-binding PA, and heparin at 10 μg/mL did not induce cytotoxicity in C2C12 cells (Figure S4 of the SI).

We then sought to compare the effect of PA nanofibers on alkaline phosphatase (ALP) activity, a marker for osteoblast differentiation (Figure 3A). Based on our dose-response pilot for the effect of BMP-2-mediated C2C12 differentiation into osteogenic cells (Figure S5 of the SI), 50 ng/mL BMP-2 was selected as a fixed treatment condition for our *in vitro* studies. As reported previously by Zhao *et al*. [36], enzymatic labeling revealed a directly proportional association of the number of ALP-positive cells with heparin concentrations up to 10 μg/mL (Figure 3B, *top row*). We also observed an increased number of ALP-positive cells when treated with the diluent PA, which lacks the protein-binding moiety (Figure 3B, *second row*). Treatment with exogenous BMP-2 in the presence of the BMP-2-binding PA also showed a slight increase in the number of ALP-positive cells at 10 μg/mL PA concentration (Figure 3B, *third row*). Interestingly, we observed that the diluted BMP-2-binding PA exhibited the highest increase in the number of ALP-positive cells after 3 days of treatment (Figure 3B, *bottom row*). We then quantified the ALP activity of C2C12 cells and observed that all PA systems significantly increased ALP activity at 1 and 10 μg/mL in comparison to BMP-2 alone (Figure 3C). At a dose of 10 μg/mL, the diluted BMP-2-binding PA resulted in significantly higher ALP activity than heparin ($P < 0.05$), as well as the diluent PA or the BMP-2-binding PA alone ($P < 0.01$). Without the presence of BMP-2, we observed that PAs and heparin did not promote ALP expression in these cells (Figure 3D). Furthermore, we tested a PA similar in design to the diluent PA but with positively charged lysine residues, and we did not observe any enhancement of BMP-2-induced ALP activity at the same PA concentration range (Figure S6 of the SI). Overall, we observed that the negatively charged residues on the PA molecules played a crucial role in augmenting BMP-2-induced osteoblast differentiation and the addition of the BMP-2-binding epitope at an appropriate density further enhanced the potency of the growth factor.

In order to further assess the effect of PA systems on BMP-2 activity, we examined changes in the expression of osteogenic genes in C2C12 cells, including *Runx2*, *Osterix* (*Osx*), and *osteocalcin* (*Ocn*) (Figure 3E). The mRNA levels from treatments with BMP-2 in combination with the diluent PA, the BMP-2-binding PA, the diluted BMP-2-binding PA, and heparin at 10 μg/mL led to enhanced osteoblastic differentiation relative to BMP-2 alone. The diluted BMP-2-binding PA system showed the highest increase in *Runx2*, *Osx*, and *Ocn* relative to growth factor alone ($P < 0.001$). Furthermore, the diluted BMP-2-binding PA led to gene expressions that were significantly higher ($P < 0.05$) than the BMP-2-binding PA or diluent PA alone.

2.3. PA nanofiber gel prolongs growth factor retention

In order to develop therapeutic materials to promote bone regeneration, we tested the ability of the BMP-2-binding PA system to form gels and studied their BMP-2 release kinetics (Figure 4). Since the BMP-2-binding PA when used alone showed the least enhancement of BMP-2-induced activity in C2C12 cells, only the diluted BMP-2-binding PA and the diluent PA were further characterized. Indeed, both PAs were able to form self-supporting gels upon mixing with calcium chloride solution (Figure 4A). Scanning electron microscopy (SEM) verified the presence of nanofibers in these gels (Figure 3B). Rheological analysis confirmed that both PAs at 10mg/mL (or 1 wt%) exhibited gel-like properties with storage moduli (G') approximately one order of magnitude higher than the loss moduli (G”) across the tested frequency range of 1–100 s^{-1} (Figure 3C). When comparing the two PA systems, the diluted BMP-2-binding PA had G' and G” values that were lower than those of the diluent PA, respectively. BMP-2 release from these PA gels was evaluated via ELISA (Figure 3D). Upon initial loading of 50 ng BMP-2, we observed comparable loading efficiencies in the diluted BMP-2-binding PA gel, the diluent PA gel, and a conventional absorbable collagen sponge: 99.0%, 99.5%, and 98.4%, respectively. Over time, we observed a prolonged retention of the cytokine from both PA gels in comparison to the collagen sponge. After 28 days *in vitro*, the amount of BMP-2 released from the collagen sponge was approximately 4.2 ± 0.3 ng, which was more than double the amount of protein released from the diluted BMP-2-binding PA gel (1.6 ± 0.1 ng) and the diluent PA gel (1.3 ± 0.1 ng). Furthermore, we tested the ability of the PA gels to capture the growth factor from the medium that contained 25 ng BMP-2 (Figure 3E). After 4 h *in vitro*, the amount of BMP-2 bound on the diluted BMP-2-binding PA gel (15.5 ± 5.5 ng) was significantly greater than that on the diluent PA gel (6.4 ± 0.7 ng). After 16 h, we found no significantly difference in the amount of growth factor bound on the two gels.

2.4. BMP-2-binding PA gel augments spinal fusion

In order to verify *in vivo* the efficacy of the BMP-2-binding PA to promote BMP-2-induced osteogenesis and to identify the ideal proportions of the binding and diluent PAs, we utilized a mouse muscle pouch model to assess ectopic bone formation following implantation of various gel formulations impregnated with 1 μg BMP-2. After 2 weeks, radiographs revealed that the 50%-diluted BMP-2-binding PA gel exhibited new bone that was qualitatively more localized and larger in size than those formed by the 10%-diluted BMP-2-binding PA gel or the 100% BMP-2-binding PA gel (Figure S7 of the SI).

With the objective of investigating the translational potential of the supramolecular nanofibers, we evaluated next the ability of the BMP-2-binding PA system to promote bone formation and spine arthrodesis in a well-established rat posterolateral lumbar intertransverse spinal fusion model (Figure 5). In this model the bone healing process is initiated at the fusion bed site between L4 and L5 transverse processes [38,39]. Based on both *in vitro* as well as the ectopic bone formation results, the 50%-diluted BMP-2-binding PA was selected as the treatment condition for the spinal fusion study. Hence, the diluted BMP-2-binding PA gel, the diluent PA gel, and the collagen sponge were preloaded with BMP-2 doses of 0, 0.1, to 1 μg per animal and applied to bridge the decorticated L4 and L5 transverse processes (Table 1). Eight weeks post-treatment, blind manual palpation scores demonstrated that treatments with the diluted BMP-2-binding PA gel elicited the highest fusion scores relative to other conditions with equivalent doses of BMP-2 (Figure 5A). We observed that the diluted BMP-2-binding PA with 1 μg BMP-2 was the only treatment that showed an average fusion score (2.4 ± 0.0) that was comparable to treatment with 10 μg BMP-2 in collagen sponge (clinical positive control; 2.2 ± 0.1). When preloaded with 1 μg BMP-2, the diluted BMP-2-binding PA gel resulted in a significantly higher fusion score ($P < 0.001$) than the diluent PA gel (1.4 ± 0.2) or collagen sponge (1.0 ± 0.2). At 0.1 μg BMP-2, the diluted BMP-2-binding PA gel elicited an average fusion score (0.6 ± 0.2) was significantly higher ($P < 0.01$) than the effectively zero fusion score for a collagen sponge. At this dose of growth factor, the average fusion score of the diluent PA gel (0.4 ± 0.1) was also significantly higher ($P < 0.05$) than that of the collagen sponge. Remarkably, we observed that the diluted BMP-2-binding PA gel alone without any exogenous growth factor elicited a significantly greater fusion score (0.6 ± 0.2) than the other treatments ($P < 0.05$).

Fusion rates followed the same trend from average fusion scores, with the diluted BMP-2-binding PA gel generally outperforming the other treatments at all doses of BMP-2 (Figure 5B). When preloaded with 1 μg BMP-2, the collagen sponge, the diluent PA gel, and the diluted BMP-2-binding PA gel elicited fusion rates of 67%, 75%, and 100%, respectively. It is notable that the 100% fusion rate seen with 10 μg BMP-2 on collagen sponge (positive control) was achievable with only 1 μg BMP-2 when delivered in the diluted BMP-2-binding PA gel. With 0.1 μg BMP-2, both the collagen sponge and diluent PA gel resulted in fusion rates of 0%, whereas the diluted BMP-2-binding PA gel resulted in a fusion rate of 33%. Interestingly, as seen in the fusion score analysis, we observed a 42% fusion rate when treated with the diluted BMP-2-binding PA without the addition of BMP-2.

In order to quantify the amount of new bone formed in the transverse processes, we performed quantitative analysis of μCT reconstructions of the samples that were successfully fused (Table 1). In all of the conditions, the diluted BMP-2-binding PA gel with 1 μg BMP-2 had by far the highest mean volume of new ossified tissue (460.6 ± 65.3 mm^3) relative to all other treatments (Figure 5C). This mean volume was significantly greater ($P < 0.001$) than those observed in animals treated with 1 μg BMP-2 in the diluent PA gel (112.7 ± 41.4 mm^3) or in the collagen sponge (135.9 ± 15.9 mm^3) by at least a factor of three. In addition, treatment with 0.1 μg BMP-2 delivered in the diluted BMP-2-binding PA gel exhibited on average new bone volume (162.1 ± 54.5 mm^3) that was similar to those treated with BMP-2 at a dose ten-fold higher (10 μg) in the diluent PA gel or the collagen sponge.

Following the trend from the manual palpation analysis, we also observed by μCT evaluation the presence of new bone formed by the diluted BMP-2-binding PA gel that had no exogenous BMP-2 (212.2 ± 58.2 mm^3), and this mean volume was comparable to those in animals treated with either the diluent PA gel or collagen sponge at all doses of BMP-2. Representative images from 3-D μCT rendering revealed that in all of the animals with successful fusion, the diluted BMP-2-binding PA gel was the only treatment that exhibited some degree of bilateral bridging of the L4 and L5 transverse processes at all BMP-2 doses, including the 0 μg dose (Figure 5D). Dorsal-ventral radiographs of these samples taken at 8 weeks post-treatment verified fusion observed in μCT rendering (Figure S8 of the SI).

Histological analysis of spine specimens, using hematoxylin and eosin staining, confirmed the results from μCT measurements (Figure 6). Treatment with the diluted BMP-2-binding PA in the presence of 1 μg BMP-2 demonstrated robust fusion mass, and the cortical trabeculae from this sample was thicker and more abundant when compared to other groups containing 1 μg BMP-2. No evidence of a local inflammatory response was found in any of the specimens.

3. Discussion

We have demonstrated in this work the use of supramolecular nanofibers as a promising strategy to promote osteogenesis in spinal fusion. The BMP-2-binding PA showed enhanced BMP-2-induced osteoblast differentiation *in vitro*, and when prepared as a gel it exhibited prolonged retention of the growth factor. Our evaluation of this bioactive nanofiber gel in a rat posterolateral lumbar intertransverse spinal fusion model revealed a 100% fusion rate with increased bone formation when loaded with a BMP-2 dose ten-fold lower than that required for sufficient arthrodesis using a collagen sponge. Most importantly, a 42% spinal fusion rate was also achieved with the nanofiber gel alone without the addition of exogenous BMP-2. Overall, the efficacy demonstrated here supports the use of this PA system as a translatable approach to improve upon or even perhaps replace current clinical modes of BMP-2 use in the treatment of degenerative disc diseases and other spinal disorders.

Heparan sulfate-like glycosaminoglycans (HSGAGs), rich in sulfo- and carboxyl-groups, are known to potentiate osteogenesis induced by BMP-2 *in vitro* [40,41] and *in vivo* as well [36,37]. We have shown here that supramolecular nanofibers containing BMP-2-binding peptide sequences can mimic certain aspects of the natural polysaccharides and augment the BMP-2-induced osteoblast differentiation of C2C12 myoblasts *in vitro*. Our results also revealed that negatively charged diluent PA nanofibers can also enhance the BMP-2-induced osteoblast differentiation as measured through the increased ALP activity and expression of other osteogenic gene markers. Since BMP-2 is a basic growth factor with an isoelectric point near 9.0 [42], it is possible that the carboxyl residues on the nanofiber surface can bind BMP-2 by electrostatic attraction and exhibit heparin-like features which result in cell signaling. Also, we were able to verify the importance of the electrostatic attraction between the basic protein and the acidic PA by using a basic PA, which failed to enhance BMP-2-induced osteoblast differentiation of C2C12 cells (Figure S6 of the SI). Furthermore, when this diluent PA was co-assembled with the BMP-2-binding PA at 1:1 weight ratio, the resulting supramolecular nanofiber system exhibited greater enhancement of BMP-2 activity

in comparison to either PA alone. In a previous investigation from our laboratory, we found that a PA bearing a cell adhesion epitope (RGDS) promoted optimal cell adhesion when diluted to 10% with diluent PAs lacking the epitope [43]. We therefore hypothesize here that the dilution of the BMP-2-binding PA results in enhanced display of the binding sequences on the nanofiber surface, thus facilitating optimal binding interactions between the peptide sequence and BMP-2.

Similar to PA systems that have been investigated previously as therapeutic gels with controlled growth factor release [21,27,28,44], we also observed in this study that the diluted BMP-2-binding PA gel and the diluent PA gel showed BMP-2 release rates that were much slower than the burst release observed from the absorbable collagen sponge. In addition, there was no significant difference in the release profiles between the two PA nanofiber gels after 28 days at physiological pH; the diluent PA gel even exhibited better BMP-2 retention than the diluted BMP-2-binding PA gel during the first 10 days. This is in contrast to the SPR analysis, which showed that the BMP-2-binding PA had a greater binding affinity to BMP-2 than the diluent PA. However, due to the non-specific interactions between the PA nanofibers and the NTA-dextran substrate at pH 7.4, the SPR analysis was performed at pH 8.4 where there was minimal PA supramolecular assembly. Therefore, in the bulk PA gels, it is possible that the high charge density on the surface of the diluent PA nanofibers may elicit electrostatic binding to BMP-2 that was not captured by the SPR analysis. In this context, we have previously observed that a gel made of the diluent PA nanofibers exhibited a very strong binding to several growth factors and this binding was diminished when the PA was co-assembled at 10 mol% level with a different PA which decreased its surface charge density. However, when we co-assembled the diluent PA with the BMP2-binding PA, we did not observe the expected decrease in protein retention ability. This indicates that it is the BMP-2-binding epitope that is responsible for maintaining the same protein release profile even though the charge density has not been diminished. Interestingly, we observed a difference between these two PA gels in their abilities to capture the growth factor from the medium. After a 4 h incubation period, the diluted BMP-2-binding PA gel captured more BMP-2 than the diluent PA; however, BMP-2 captured by the two gels was comparable by 16 h. Since the BMP-2-binding PA exhibited a greater binding affinity to BMP-2 than the diluent PA in the SPR analysis, it is possible that the bioactive epitope is able to capture the growth factor faster during the early incubation period. However, the non-specific, electrostatic binding of BMP-2 by the diluent PA is accumulated over time, resulting in comparable amounts of BMP-2 captured by the two gels.

Effective spinal arthrodesis in the model utilized here is known to occur with the use of a collagen sponge containing 10 μg BMP-2 [11,38]. In contrast the diluted BMP-2-binding PA gel investigated here led to 100% fusion rate with a high probability of bilateral bridging using only 1 μg BMP-2, thus reducing the required growth factor dose by 10-fold. On the other hand, the diluent PA gel with the same growth factor dose (1 μg) elicited a fusion rate of 75%. The difference in fusion rates between these two nanofiber systems suggests that the therapeutic efficacy observed with the BMP-2-binding PA is not only due to a prolonged retention of the cytokine within the bulk gel, but also due in part to the inherent bioactivity of the nanofibers. We hypothesize that once mesenchymal stem cells make contact with or enter the PA gels, the presentation of BMP-2 by the BMP-2-binding nanofibers within the

microenvironment potentiates protein signaling and promotes an enhanced osteogenesis. While this mechanism is strongly suggestive by our results, more work is needed to investigate the recruitment of progenitor cells *in vivo*.

We have also demonstrated a 42% spinal fusion rate with the use of the BMP-2-binding PA without any exogenous growth factor, whereas the diluent PA or collagen sponge did not show an innate ability to induce fusion. The average fusion mass volume by the bioactive PA was comparable to those treated with 1 μg BMP-2 incorporated in the diluent PA gel or the collagen sponge. These results suggest that the amount of endogenously expressed BMP-2 at the fusion bed site may be sufficient to promote osteogenesis in the presence of the bioactive nanofiber networks with specific protein-binding capacity. Similarly, heparan sulfate chains that are affinity-matched to BMP-2 have been reported to promote bone regeneration in a rabbit critical-size ulnar defect model by harnessing endogenously produced BMP-2 [45].

4. Conclusions

We have demonstrated that self-assembling PA nanofibers with binding affinity for BMP-2 are effective in eliciting arthrodesis in a rat posterolateral lumbar intertransverse spinal fusion model. This BMP-2-binding PA system allowed a ten-fold reduction in the BMP-2 dose necessary to achieve 100% fusion rate, and also promoted a spinal fusion rate of 42% without exogenous BMP-2. We propose that the observed efficacy in this translational model of bone regeneration is linked to the ability of the BMP2-binding nanofibers to potentiate osteogenesis signaling of both exogenously delivered and endogenously expressed growth factor. The bioactive nanofiber system is a promising approach to bone grafting for spine fusion without the undesirable side effects of high supraphysiologic doses of BMP-2.

5. Experimental Section

Materials

C2C12 myoblast cell line and DMEM were purchased from American Type Culture Collection (ATCC, Manassas, VA). C2C12 cells were used at passages 3 to 6. Heat inactivated HyClone fetal bovine serum (FBS) was purchased from Thermo Scientific (Hanover Park, IL). Commercial porcine mucosa-derived heparin sodium was purchased from Celsus Laboratories (Cincinnati, OH). Recombinant human BMP-2 was obtained from Medtronic Sofamor Danek (Minneapolis, MN).

PA synthesis and preparation

All PAs were synthesized using standard 9-fluorenyl methoxycarbonyl (Fmoc) solid-phase peptide synthesis and purified by reverse phase high performance liquid chromatography (HPLC) in a water-acetonitrile gradient, each containing 0.1% v/v ammonium hydroxide (NH_4OH). PAs were synthesized with the following amino acid sequences and a carbon alkyl tail covalently attached: C_{12}-(K)$V_3A_3E_3$-SGGGYPVHPST-NH_2 (BMP2b-PA) and C_{16}-$V_3A_3E_3$-COOH (diluent PA) [21,32]. Purified PA was stored at −20°C until use. For all studies, lyophilized BMP2b-PA and diluent PA were separately reconstituted in sterile 2

mM NH_4OH at desired concentrations (wt%) and sonicated for 30 min. In order to space BMP-2-binding segments on the surface of the supramolecular nanofibers, the diluted BMP2b-PA (D-BMP2b-PA) was prepared by mixing equal volumes of BMP2b-PA and diluent PA at equal concentrations, followed by 30 min sonication; the final PA concentration of D-BMP2b-PA therefore remained the same as prior to mixing. All PAs were freshly dissolved for each experiment.

Circular dichroism (CD)

CD was performed on a J-815 CD spectrophotometer (Jasco, Easton, MD). PA samples were prepared at 1 wt%, then diluted to 0.01 wt% in 0.1 mM $CaCl_2$. Measurements were collected at 37°C over a wavelength range of 280–180 nm with a 0.5 nm step size and five accumulations per scan.

Cryogenic transmission electron microscopy (cryo-TEM)

Cryo-TEM was performed on a JEOL 1230 microscope (JEOL USA, Peabody, MA) according to a previously described protocol [22]. PA samples were prepared at 1 wt%, then diluted to 0.5 wt% in 0.1 mM $CaCl_2$ for imaging.

Surface plasmon resonance (SPR) measurements

The SPR measurements were performed using a Biacore 3000 instrument (GE Healthcare, Pittsburg, PA) equipped with a NTA Sensor Chip (GE Healthcare) at 25°C. HBS-P eluent buffer and HBS-EP dispenser buffer were purchased from GE Healthcare. $NiCl_2$ solution (500 μM in eluent buffer), elution buffer (300 mM imidazole and 500 mM NaCl in water), and regeneration buffer (10mM HEPES, 150 mM NaCl, 0.005% polysorbate 20, 350 mM EDTA at pH 7.4) were prepared according to Biacore specifications. Human recombinant BMP-2 with hexahistidine-tag fused at the C-terminus (AdipoGen, San Diego, CA) was initially reconstituted in PBS at 20 μg/mL, and diluted to 500 nM in eluent buffer.

Binding experiments were performed according to a previously described protocol [35]. Ni^{2+} was first loaded on the NTA chip for 5 min at a flow rate of 20 μL/min, and then His-BMP-2 for 1.25 min at 4 μL/min. Afterwards, each PA sample was injected for 2 min at 20 μL/min, followed by 5 min dissociation at 20 μL/min. The flow cell was regenerated using the elution buffer and the regeneration buffer, each for 2 min at 100 μL/min. The surface was further washed with 0.5% SDS in water for 12 sec at 100 μL/min. PA samples were horn-sonicated and diluted in eluent buffer that was adjusted to pH 8.5 to prevent non-specific binding to NTA. PA solutions were injected to a blank NTA flow cell without Ni^{2+} or His-BMP-2 was used as a reference cell. To compare binding affinity of the PAs, the sensograms were processed and analyzed with BIAevaluation 4.1 software. The sensogram from blank injection was subtracted from the PA sensograms, and the apparent equilibrium dissociation constant K_D was determined using 2:1 binding model, which assumes bivalent analyte interaction with two dissociation constants $k_{d,1}$ and $k_{d,2}$, where $k_{d,1}$ is more dominant.

Cell culture

C2C12 pre-myoblasts were maintained and treated with BMP-2 as depicted in Fig. 2A [36,37]. Briefly, C2C12 cells were seeded at 2×10^4 cells/cm^2 in 24-well plates in growth

media (DMEM with 10% heat-inactivated FBS and 100 U/mL penicillin/streptomycin, P/S) 1 day before treatment. On the following day (Day 0), growth media was replaced with 900 μL maintenance media (growth media with 2.5% FBS) and 100 μL treatment media containing BMP-2 with heparin or PAs. Preparation of the treatment media was as follows: 2.5 μL of BMP-2 stock (20 μg/mL) was mixed with 5 μL of heparin or PA stock solutions (0.02, 0.2, or 2 mg/mL), incubated for 5 min on ice, then mixed with DMEM (100 U/mL P/S) to a final volume of 100 μL, followed by 5 min incubation on ice. For treatments with BMP-2 only, the treatment media was prepared according to the method described except without heparin or PAs. Final working concentrations were 50 ng/mL BMP-2 and a range of 0.1, 1, to 10 μg/mL heparin or PAs.

Alkaline phosphatase (ALP) stain

The presence of ALP was stained as a marker for osteoblast differentiation on day 3 by enzymatic labeling described by Mason and Woolston [46]. Briefly, C2C12 cell layer was fixed with 4% paraformaldehyde (PFA) for 30 s, washed with PBS three times, and stained for 1 h with Naphthol AS-MX phosphate (Sigma-Aldrich, St. Louis, MO) and Fast Blue BB salt (Sigma-Aldrich) in 0.1M Tris-HCl at pH 8.2, followed by washing with PBS.

Alkaline phosphatase (ALP) activity assay

ALP activity from C2C12 cell layer was measured using QUANTI-Blue ALP substrate (InvivoGen, San Diego, CA). On Day 4, C2C12 cell monolayers were lysed on ice with 100 μL lysis buffer (20 mM Tris-HCl, 1 mM EDTA, 150 mM NaCl, 1 mM $MgCl_2$, 1% NP-40 (Igepal), and 5% glycerol at pH 7.9) containing Halt Protease Inhibitor Cocktail (Thermo Scientific). Supernatants were collected into a sterile centrifuge tube and spun at 13,200 rpm on microcentrifuge at 4 °C for 3 min. Afterwards, 20 μL of the supernatant was placed into a flat-bottom 96-well plate and mixed with 180 μL QUANTI-Blue ALP substrate (in duplicates). The plate was incubated at 37 °C for 18 h and absorbance was measured at 630 nm on SpectraMax M5 Microplate Reader (Molecular Devices, Sunnyvale, CA). In addition, 5 μL of the collected C2C12 cell supernatant was diluted with 95 μL TE buffer and mixed with 100 μL Quant-iT PicoGreen dsDNA reagent (Invitrogen) in a clear-bottom, black 96-well plate to measure the concentration of dsDNA (in triplicate). The absorbance values from QUANTI-Blue ALP assay was normalized by the amount of dsDNA in each sample, and the resulting values from heparin and PA treatments were normalized to control (BMP-2 only) to represent the relative fold increase (n=3, in triplicate experiments).

Real-time PCR

C2C12 cells were treated with 50 ng/mL BMP-2 in the presence of 10 μg/mL heparin or PAs until Day 2, and the osteogenic gene expression levels were determined by real-time PCR as described by Zhao *et al.* (n=4, in triplicate experiments) [36]. Briefly, total RNAs were isolated from cells using TRIzol (Invitrogen) and reverse-transcribed using iScript Reverse Transcription Supermix (Bio-Rad, Des Plaines, IL). PCR amplification was analyzed with iQ5 Real-Time PCR Detection System (Bio-Rad) using iQ SYBR Green Supermix (Bio-Rad) and the following primers: *Runx2* types II & III (*Runx2*), 5'-ATGCTTCATTCATTCGCCTCACAAAC-3' and 5'-CCAAAAGAAGCTTTGCTG-3';

Osterix (*Osx*), 5'-TTAAGCTTGCGTCCTCTCTGCTTGA-3' and 5'-TTTCTAGATCAGATCTCTAGCAGGTT-3'; *Osteocalcin* (*Ocn*), 5'-CAAGTCCCACACAGCAGCTT-3' and 5'-AAAGCCGAGCTGCCAGAGTT-3'; and *Glyceraldehyde-3-phosphate dehydrogenase* (*GAPDH*), 5'-TGAAGGTCGGTGTGAACGGATTGGC-3' and 5'-CATGTAGGCCATGAGGTCCACCAC-3' (IDT, Coralville, IA). For PCR amplification, cDNA was denatured at 94°C for 5 min, then underwent 40 repeated cycles at 94°C for 45 s, annealing at 55°C for 1 min, and extension at 68°C for 1 min, followed by 79 repeated cycles at 55°C for 30 s for generation of a melting curve. Expression values of *Runx2 II*, *Osx*, and *Ocn* were normalized to the respective *GAPDH* levels, and all treatments were normalized to control (BMP-2 only) treatment in order to represent relative fold increase.

PA nanofiber gel assembly

Diluent PA, BMP2b-PA, and D-BMP2b-PA solutions were prepared at 2 wt%. PA gel (1 wt % PA) was formed by mixing equal volumes of 2 wt% PA and 20 m_M $CaCl_2$. Where recombinant human BMP-2 was incorporated into the PA gel, the protein was first combined with 20 m_M $CaCl_2$ solution prior to mixing with PA.

Scanning electron microscopy (SEM)

PA nanofiber gels were fixed in 4% paraformaldehyde, dried, then visualized with a Hitachi S-4800 II FE-SEM (Hitachi High Technologies America, Dallas, TX) according to a previously described protocol [28].

Rheology

Rheological measurements were performed using MCR-300 rheometer (Anton Parr, Graz, Austria) with a 25 mm parallel plate at 0.5 mm gap distance and 37°C stage temperature. To initiate gel formation, 20 μL of 0.2 $_M$ $CaCl_2$ was added to 140 μL of 1.25 wt% PA solution on the rheometer plate. After a 30 min equilibration period at 37°C, the samples were tested at a constant strain of 0.5% over angular frequency range of 1–100 s^{-1} (n=3).

Growth factor release kinetics from PA gels

Absorbable collagen sponges cut to 0.135 cm^3 as measured using digital microcalipers with a resolution of 0.01 mm were placed into microfuge tubes and pre-loaded with 50 ng of recombinant human BMP-2. Both the diluted BMP-2-binding PA gels and the diluent PA gels were prepared to a final volume of 40 μL with 50 ng of BMP-2 as described above. After a 20 min incubation period, 700 μL of release media (0.1% BSA in PBS) was applied to each tube. Tubes were pulse-spun, and 300 μL of release media was collected from each. An additional 300 μL of fresh release media was applied to the scaffolds, and the tubes were pulse-spun. The second 300 μL aliquot of release media was collected from each tube and combined with the original aliquot to obtain a 600 μL supernatant sample at day 0. A final addition of 300 μL fresh release media was applied to each tube, and scaffolds were incubated at 4°C until the next time point. At increasing time points out to 28 days, the same procedure was performed, with two aliquots of release media removed for future analysis and fresh media subsequently replaced. All aliquots were frozen at −80°C until quantitation.

BMP-2 was quantified in the collected samples using a sandwich ELISA (R&D Systems, Minneapolis, MN) per the manufacturer's instructions.

Growth factor capture by PA gels

Both the diluted BMP-2-binding PA gels and the diluent PA gels were prepared as described above to a final volume of 20 μL inside a 2 mL microcentrifuge tube. After a 10 min incubation period, 1 mL of 25 ng/mL BMP-2 media (0.01% BSA in DMEM) was applied. Tubes were gently inverted ten times and incubated at 37°C. At each time point (4 and 16 h), the tubes were inverted twice and media was collected and stored at −80°C until quantitation. Separate gels were made for each time point. BMP-2 was quantified using a sandwich ELISA.

Rat posterolateral lumbar intertransverse spinal fusion

This study was approved by the Institutional Animal Care and Use Committee and was conducted in line with IACUC policies and procedures. One hundred and twelve female Sprague-Dawley rats at ages 12–16 weeks were utilized (Table 1). Control groups consisted of 0 μg BMP-2 per animal in collagen sponges (negative control), and 10 μg BMP-2 per animal in collagen sponges (positive control; fuses at a rate of 100% in this model) [38,47]. Animals were first assigned to one of three treatment groups: the diluted BMP-2-binding PA gels, the diluent PA gels, or the collagen sponge. Each treatment was further divided into sub-groups with varying BMP-2 doses of 0, 0.1, and 1 μg per animal, which have been shown previously *not* to reliably fuse the spine when applied on a collagen sponge in this model [38]. In all conditions, the denoted BMP-2 dose refers to total growth factor dose implanted per animal. For instance, in the 1 μg BMP-2 treatment group, two biomaterials were each impregnated with 0.5 μg BMP-2 and implanted adjoining the L4–L5 transverse processes on either side of the spine. Each PA gel was prepared at 100 μL for each side of the spine.

Surgical procedures

Rats were maintained on a heating pad under continuous anesthesia with an isoflurane inhalational anesthetic delivery system, and they were monitored by an assistant for cardiac or respiratory difficulties throughout the procedure. Utilizing a previously-described surgical technique, a posterior midline incision was made over the lumbar spinous processes, after which two separate fascial incisions were made 4 mm from the midline [39]. The L4 and L5 transverse processes were exposed using a muscle-splitting approach via blunt dissection down to the periosteum. After adequate exposure, the fusion bed was irrigated with sterile gentamicin/saline solution, and a high-speed burr was used to decorticate the superficial cortical layer of the transverse processes. Graft materials were then implanted bilaterally in the paraspinal musculature between the transverse processes. The fascia and skin incisions were closed using a simple interrupted pattern with a 3–0 Monocryl absorbable suture, which was removed from the skin 7–10 days post-surgery. Following surgery, rats were housed in separate cages and allowed to eat, drink, and bear weight *ad libitum*.

Manual palpation

Fusion was assessed via manual palpation following euthanasia at 8 weeks post-surgery. Spines were scored by three blinded observers using a previously established scoring system: 0 = no bridging; 1 = unilateral bridging; 2 = bilateral bridging; and 3 = bilateral bridging with abundant bone [39]. Spines that received an average score of 1.0 or greater were considered successfully fused.

Micro-computed tomography analysis

Specimens deemed by manual palpation as successfully fused were subject to three-dimensional μCT analysis to compare the amount of new bone formed in the transverse processes, using a Skyscan 1172 Microtomograph System (Bruker MicroCT, Kontich, Belgium). In addition, 3 control specimens without a fusion mass were analyzed and averaged to determine the host bone volume. As previously described [39], two spines were placed in a plastic holder and scanned simultaneously with the spines' axes parallel to the rotation axis of the scanner. The microfocus x-ray tube was operated at 59 kVp and 167 μA, with an exposure time of 316 ms. MicroCT scans were performed with 34.5 μm isotropic volume elements (voxels), and a mean of 777 (range: 523–849) contiguous slice data sets encompassed the L4 and L5 transverse processes.

Using ImageJ software analysis tools (NIH, Bethesda, MD) the amount of newly formed bone was quantified between the L4 and L5 transverse processes utilizing axial images for each specimen. Regions of interest (ROI) were manually defined in each slice and included the two posterolateral intertransverse fusion beds of each spine. Within the ROI, voxels more absorbing than a pre-defined threshold were identified as bone. Total bone was then calculated by adding values for each image in the fusion bed. The threshold of 450 mg/cm^3 was selected by examining several specimens and selecting the value best reproducing the structure of newly formed bone, as seen in the gray scale reconstructions. The host bone volume in the L4 and L5 transverse processes was quantified in the 3 control animals outside of the study groups and averaged (256 ± 24 mm^3). The volume of new bone formed for each spine was calculated by subtracting the mean host bone from total bone volume in each specimen.

Histology

Histology was performed as we have previously described [39]. After detachment of surrounding soft-tissue, spine specimens were fixed in 10% neutral-buffered formalin, decalcified in HCl/EDTA, and embedded in paraffin. Serial sagittal 5 μm cuts were made along the transverse processes of L4 and L5 and stained with hematoxylin and eosin.

Statistics and data analysis

For the *in vitro* cell culture study, data were analyzed using a one-way analysis of variance (ANOVA) with a Newman-Keuls multiple comparison post-hoc test. Statistical analysis was performed with the aid of Prism v5.0a. For spinal fusion study, manual palpation scores and microCT data were evaluated using a one-way ANOVA with a Levine's F test for equality of

variances and independent t test for equality of means with the aid of SPSS. In all studies, statistical significance was accepted with $P < 0.05$.

Supplementary Material

Refer to Web version on PubMed Central for supplementary material.

Acknowledgements

This work is funded by NIH/NIDCR (Grant No. 5R01DE015920-07) and DARPA (Grant No. W911NF-09-1-0044). S.S.L. is supported by Samsung Scholarship Foundation Graduate Fellowship. The following facilities at Northwestern University were used: Peptide Synthesis Core and Equipment Core at the Institute for BioNanotechnology in Medicine, EPIC Facilities of the NUANCE Center, Center for Comparative Medicine, Pathology Core Facility, Mouse Histology & Phenotyping Laboratory, and Cell Imaging Facility. The Biophysics Core Facility at the University of Chicago was also used. The authors thank Mark Seniw for his assistance with molecular graphics, Dr. Elena Solomaha for help with SPR measurements, Dr. Job Boekhoven and John Kinol for help with CMC measurements, Dr. Steve Strathmann (Baxter) for microCT scanning, and John Nelson for help with spine specimen histology. Authors also thank Dr. Liam Palmer, Dr. Nicholas Stephanopoulos, and Dr. Jack Donners for useful discussions. Furthermore, the authors thank Dr. Chrstina Newcomb, Dr. Stuart Stock, and Dr. David Wellman for their assistance in the preliminary animal study.

References

[1]. Hsu WK, Nickoli MS, Wang JC, Lieberman JR, An HS, Yoon ST, Youssef JA, Brodke DS, McCullough CM. Global Spine J. 2012; 02:239. [PubMed: 24353975]

[2]. Aghdasi B, Montgomery SR, Daubs MD, Wang JC. Surgeon. 2013; 11:39. [PubMed: 23040457]

[3]. Latham W, Lau JTC. Techniques in Orthopaedics. 2011; 26:14.

[4]. Reddi AH. Nature Biotechnology. 1998; 16:247.

[5]. Brower RS, Vickroy NM. Spine. 2008; 33:E653. [PubMed: 18708918]

[6]. Muchow RD, Hsu WK, Anderson PA. Spine J. 2010; 10:e1. [PubMed: 20797648]

[7]. Vaidya R, Sethi A, Bartol S, Jacobson M, Coe C, Craig JG. J Spinal Disord Tech. 2008; 21:557. [PubMed: 19057248]

[8]. Wong DA, Kumar A, Jatana S, Ghiselli G, Wong K. The Spine Journal. 2008; 8:1011. [PubMed: 18037352]

[9]. Aro HT, Govender S, Patel AD, Hernigou P, Perera de Gregorio A, Popescu GI, Golden JD, Christensen J, Valentin A. J Bone Joint Surg Am. 2011; 93:801. [PubMed: 21454742]

[10]. Willie BM, Petersen A, Schmidt-Bleek K, Cipitria A. Soft Matter. 2010

[11]. Hsu WK, Polavarapu M, Riaz R, Larson AC, Diegmueller JJ, Ghodasra JH, Hsu EL. Spine. 2013; 38:E691. [PubMed: 23429681]

[12]. Lee K, Silva EA, Mooney DJ. J R Soc Interface. 2011; 8:153. [PubMed: 20719768]

[13]. Shah NJ, Hyder MN, Moskowitz JS, Quadir MA, Morton SW, Seeherman HJ, Padera RF, Spector M, Hammond PT. Sci Transl Med. 2013; 5:191ra83.

[14]. Benoit DSW, Collins SD, Anseth KS. Adv Funct Mater. 2007; 17:2085. [PubMed: 18688288]

[15]. Lutolf MP, Gilbert PM, Blau HM. Nature. 2009; 462:433. [PubMed: 19940913]

[16]. Pashuck ET, Stevens MM. Sci Transl Med. 2012; 4:160sr4. [PubMed: 23152328]

[17]. Hudalla GA, Murphy WL. Adv Funct Mater. 2011; 21:1754. [PubMed: 21921999]

[18]. Hartgerink J, Beniash E, Stupp S. Science. 2001; 294:1684. [PubMed: 11721046]

[19]. Matson JB, Zha RH, Stupp SI. Current Opinion in Solid State and Materials Science. 2011; 15:225. [PubMed: 22125413]

[20]. Tysseling-Mattiace V, Sahni V, Niece K, Birch D, Czeisler C, Fehlings MG, Stupp SI, Kessler JA. Journal of Neuroscience. 2008; 28:3814. [PubMed: 18385339]

[21]. Shah RN, Shah NA, Del Rosario Lim MM, Hsieh C, Nuber G, Stupp SI. Proceedings of the National Academy of Sciences. 2010; 107:3293.

[22]. Webber MJ, Tongers J, Newcomb CJ, Marquardt KT, Bauersachs J, Losordo DW, Stupp SI. Proceedings of the National Academy of Sciences. 2011; 108:13438.

[23]. Huang Z, Newcomb CJ, Bringas P, Stupp SI, Snead ML. Biomaterials. 2010; 31:9202. [PubMed: 20869764]

[24]. Mata A, Geng Y, Henrikson K, Aparicio C, Stock SR, Satcher RL, Stupp SI. Biomaterials. 2010; 31:6004. [PubMed: 20472286]

[25]. Sargeant TD, Guler MO, Oppenheimer SM, Mata A, Satcher RL, Dunand DC, Stupp SI. Biomaterials. 2008; 29:161. [PubMed: 17936353]

[26]. Ghanaati S, Webber M, Unger R, Orth C, Huvat JF, Barbeck M, Rasic A, Stupp SI, Kirkpatrick CJ. Biomaterials. 2009; 30:6062.

[27]. Rajangam K, Behanna HA, Hui MJ, Han X, Hulvat JF, Lomasney JW, Stupp SI. Nano letters. 2006; 6:2086. [PubMed: 16968030]

[28]. Lee SS, Huang BJ, Kaltz SR, Sur S, Newcomb CJ, Stock SR, Shah RN, Stupp SI. Biomaterials. 2012; 34:452. [PubMed: 23099062]

[29]. Capila I, Linhardt RJ. Angewandte Chemie (International ed in English). 2002; 41:391. [PubMed: 12491369]

[30]. Morgan MR, Humphries MJ, Bass MD. Nat Rev Mol Cell Biol. 2007; 8:957. [PubMed: 17971838]

[31]. Rajangam K, Arnold MS, Rocco MA, Stupp SI. Biomaterials. 2008; 29:3298. [PubMed: 18468676]

[32]. Behanna HA, Donners JJJM, Gordon AC, Stupp SI. J Am Chem Soc. 2005; 127:1193. [PubMed: 15669858]

[33]. Pashuck ET, Cui H, Stupp SI. J Am Chem Soc. 2010; 132:6041. [PubMed: 20377229]

[34]. Boekhoven J, Brizard AM, van Rijn P, Stuart MCA, Eelkema R, van Esch JH. Angewandte Chemie (International ed in English). 2011; 50:12285. [PubMed: 21761526]

[35]. Knecht S, Ricklin D, Eberle AN, Ernst B. J. Mol. Recognit. 2009; 22:270. [PubMed: 19235144]

[36]. Zhao B, Katagiri T, Toyoda H, Takada T, Yanai T, Fukuda T, Chung U-I, Koike T, Takaoka K, Kamijo R. J Biol Chem. 2006; 281:23246. [PubMed: 16754660]

[37]. Bramono DS, Murali S, Rai B, Ling L, Poh WT, Lim ZX, Stein GS, Nurcombe V, van Wijnen AJ, Cool SM. Bone. 2011; 50:954. [PubMed: 22227436]

[38]. Hsu WK, Wang JC, Liu NQ, Krenek L, Zuk PA, Hedrick MH, Benhaim P, Lieberman JR. J Bone Joint Surg Am. 2008; 90:1043. [PubMed: 18451397]

[39]. Hsu WK, Polavarapu M, Riaz R, Roc GC, Stock SR, Glicksman ZS, Ghodasra JH, Hsu EL. J Orthop Res. 2011; 29:1812. [PubMed: 21590717]

[40]. Kuo W-J, Digman MA, Lander AD. Mol Biol Cell. 2010; 21:4028. [PubMed: 20861306]

[41]. Jiao X, Billings PC, O'Connell MP, Kaplan FS, Shore EM, Glaser DL. J Biol Chem. 2007; 282:1080. [PubMed: 17020882]

[42]. Uludag H, D'Augusta D, Golden J, Li J, Timony G, Riedel R, Wozney JM. J Biomed Mater Res. 2000; 50:227. [PubMed: 10679688]

[43]. Webber M, Tongers J, Renault M, Roncalli J, Losordo D, Stupp S. Acta biomaterialia. 2010; 6:3. [PubMed: 19635599]

[44]. Angeloni N, Bond C, Tang Y, Harrington DA, Zhang S, Stupp SI, McKenna KE, Podlasek CA. Biomaterials. 2010; 32:1091. [PubMed: 20971506]

[45]. Murali S, Rai B, Dombrowski C, Lee JLJ, Lim ZXH, Bramono DS, Ling L, Bell T, Hinkley S, Nathan SS, Hui JH, Wong HK, Nurcombe V, Cool SM. Biomaterials. 2013; 34:5594. [PubMed: 23632323]

[46]. Bullock, GR.; Petrusz, P. Techniques in Immunocytochemistry. Academic Press; London: 1982. Etc

[47]. Peterson B, Whang PG, Iglesias R, Wang JC, Lieberman JR. J Bone Joint Surg Am. 2004; 86-A: 2243. [PubMed: 15466734]

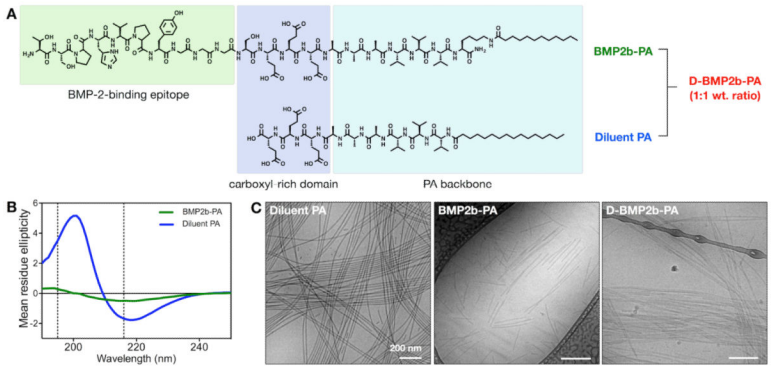

Figure 1.

Design and characterization of the BMP-2-binding PA nanofibers. (**A**) Chemical structures of the BMP-2-binding PA (BMP2b-PA) and the diluent PA, which will be mixed at equal wt.% ratio to form the diluted BMP-2-binding PA system (D-BMP2b-PA). (**B**) Circular dichroism for the BMP-2-binding PA and the diluent PA demonstrating β-sheet secondary structures. (**C**) Cryogenic transmission electron microscopy (Cryo-TEM) showing the filamentous nanostructures of the diluent PA, the BMP-2-binding PA, and the diluted BMP-2-binding PA.

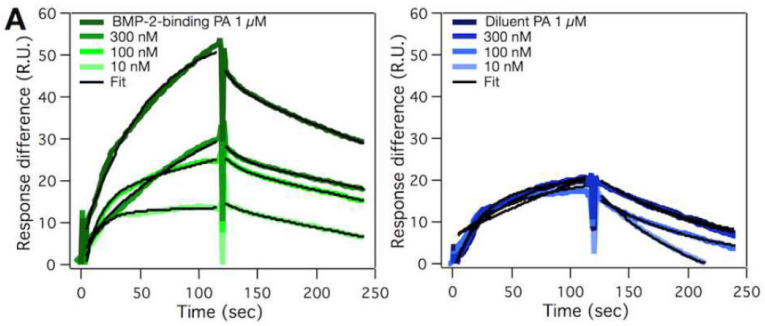

B

	$k_{d,1}$ (s^{-1})	$k_{d,2}$ (s^{-1})	R_1/R_2	k_a (M^{-1} s^{-1})	K_D (M)	*Chi2*
BMP-2-binding PA	6.9×10^{-4}	7.8×10^{-2}	41.5	1.8×10^{4}	3.7×10^{-8}	0.511
Diluent PA	1.1×10^{-2}	1.1×10^{-3}	10.2	5.3×10^{3}	2.1×10^{-6}	1.66

Figure 2.

Binding affinities of the PA systems to BMP-2 using surface plasmon resonance. (**A**) Overlay plots showing the binding of the BMP-2-binding PA (green) and the diluent PA (blue) in subsequent dilutions. The calculated fit (black) was obtained using the 2:1 binding model with constants shown in (**B**).

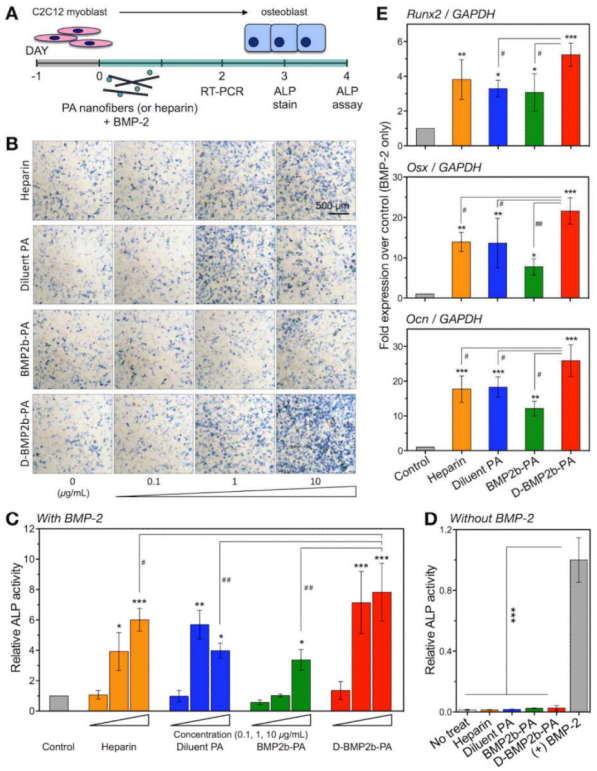

Figure 3.

BMP-2-induced osteoblast differentiation is enhanced by the BMP-2-binding PA nanofibers *in vitro*. (**A**) Schematics of C2C12 cell cultures. Cells were seeded 1 day prior to treatment. On the day of treatment (Day 0), new media was added with the addition of 50 ng/mL BMP-2 along with PAs or porcine heparin at 0, 0.1, 1 or 10 μg/mL. (**B**) Cells were stained for the presence of ALP after 3 days. A representative scale bar is shown. (**C**) ALP enzyme activity was measured after 4 days. Measurements were normalized to their respective DNA content, and the final average values from treatments are normalized to control treatment with BMP-2 alone. (**D**) ALP enzyme activity was measured after 4 days of treatment with PA or heparin at 10 μg/ml without BMP-2. Final average values are normalized to the positive control treatment containing BMP-2. (**E**) Expression of osteogenic mRNAs after 2 days: *Runx2*, *Osterix (Osx)*, and *osteocalcin* (*Ocn*). PAs and heparin were tested at 10 μg/mL with BMP-2. Each expression was normalized to GAPDH, and the average values were normalized to control treatment with BMP-2 alone. Data are means ± SD; **P* < 0.05, ***P* < 0.01, ****P* < 0.001.

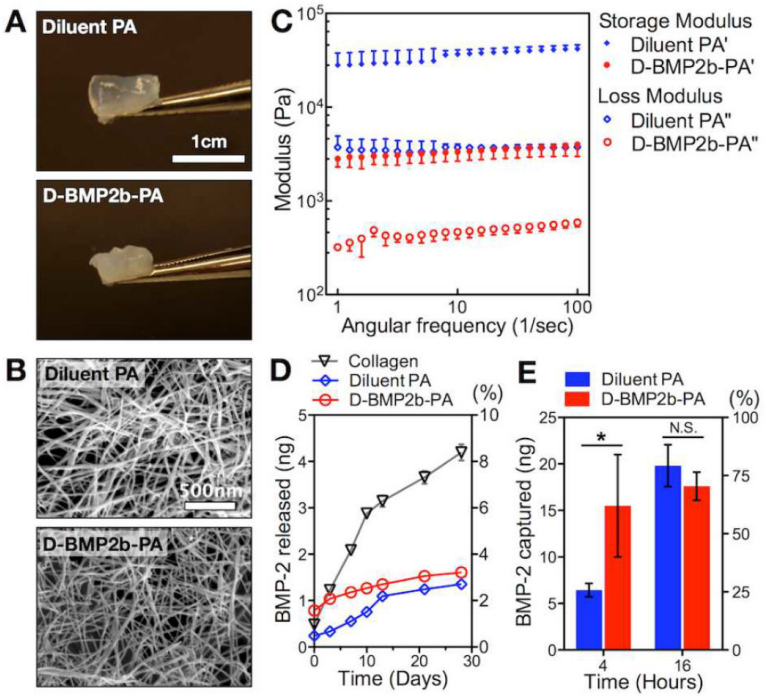

Figure 4.

Characterization of PA nanofiber gels. (**A**) Photograph of self-supporting PA gels. (**B**) Scanning electron microscopy (SEM) showing a network of filamentous nanostructures in the PA gels. (**C**) Rheological values of the diluted BMP-2-binding PA gel and the diluent PA gel at 1 wt% final concentration. Gels were equilibrated for 30 min at 37°C prior to measurement. (**D**) *In vitro* analysis of BMP-2 release from the diluted BMP-2-binding PA gel and the diluent PA gel in comparison to a bare collagen scaffold over 28 days. (**E**) *In vitro* analysis of BMP-2 capture by the diluted BMP-2-binding PA gel and the diluent PA gel at 4 and 16 hours. Data are means ± SD; **P* < 0.05.

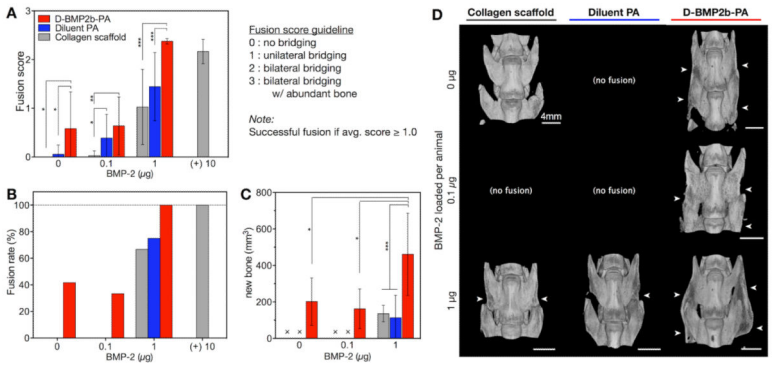

Figure 5.

BMP-2-binding PA gel promotes spinal arthrodesis in rats. Each animal received two identical graft materials with an equal dose of BMP-2 on both sides of the transverse processes. Graft materials consisted of the diluted BMP-2-binding PA gel, the diluent PA gel, or absorbable collagen sponge. The indicated dose of BMP-2 is the total per animal. (**A**) Fusion scores from blind manual palpation analysis at 8 weeks post-operation. (**B**) Fusion rates of each treatment based manual palpation scores, where an average score greater than or equal to 1.0 was considered solidly fused. (**C**) The successfully fused specimens were analyzed by microcomputed tomography (μCT) to compare fusion mass volume (mm^3). All data in this study are means ± SD; **P* < 0.05, ***P* < 0.01, ****P* < 0.001. (**D**) Representative spine reconstructions from μCT are shown for the successfully fused specimens. Scale bars shown in images. White arrows indicate the presence of fusion mass in the transverse processes.

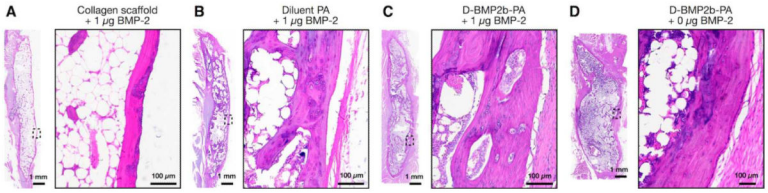

Figure 6.

Representative sagittal cross-sectional images of fused L4–L5 posterolateral spine specimens 8 weeks after surgery with hematoxylin and eosin. The box shows a higher magnification image of the inset indicated on the dorsal side of the fusion bed.

Table 1

Animal groups for the rat posterolateral lumbar intertransverse spinal fusion model study.

Treatment	*n*		
	Total	**Analyzed w/ manual palpation**	**Analyzed w/ μCT**
I. D-BMP2b-PA			
0 μg BMP-2	12	12	5
0.1 μg BMP-2	12	12	4
1 μg BMP-2	12	12	12
II. Diluent PA			
0 μg BMP-2	12	12	0
0.1 μg BMP-2	12	12	0
1 μg BMP-2	12	12	9
III. Collagen scaffold			
0 μg BMP-2	8	8	3*
0.1 μg BMP-2	12	12	0
1 μg BMP-2	12	12	8
10 μg BMP-2 (+)	8	8	0

* analyzed as threshold values for μCT analysis